applied sciences

MDPI

Article

Insight into the Preparation of MgAl-Layered Double Hydroxide (LDH) Intercalated with Nitrates and Chloride Adsorption Ability Study

Yanhui Cao [1,2,*], Shuo Fang [1,3], Kaifeng Chen [1,2], Haixia Qi [1,2], Xinyue Zhang [1,2], Congshu Huang [1,2], Jingjing Wang [1,2] and Jianchun Liu [4]

1 Luoyang Ship Material Research Institute, Xiamen 361101, China; fangshuo0220@163.com (S.F.); xm725ckf@163.com (K.C.); qihaixia19861222@126.com (H.Q.); ohtlys@sina.cn (X.Z.); hcs05@126.com (C.H.); jingjing811014@163.com (J.W.)
2 Science and Technology on Marine Corrosion and Protection Laboratory, Xiamen 361101, China
3 Liaoning Provincial Key Laboratory for Preparation and Application of Special Functional Materials, Shenyang University of Chemical Technology, Shenyang 110142, China
4 China Ship Development and Design Center, Wuhan 430064, China; liujc27@126.com
* Correspondence: yanhuicao@yeah.net; Tel.: +86-155-0692-2136

Featured Application: The synthesized MgAl layered double hydroxide (LDH) with strong chloride adsorption ability will have great application potential in the field of corrosion protection.

Abstract: In recent years, layered double hydroxide (LDH) has attracted extensive attention of researchers in the field of corrosion protection due to its unique structure and anion exchange characteristics. However, its chloride adsorption capacity remains to be further optimized to increase its corrosion protection ability. In this work, the influence of reactant concentration on the prepared MgAl-LDH intercalated with nitrates was investigated, and the morphology, composition, and structure were characterized by scanning electronic microscopy/energy dispersive spectrometer (SEM/EDS), transmission electron microscopy (TEM), Fourier transform infrared spectroscopy (FTIR), X-ray photoelectron spectroscopy (XPS), and X-ray diffraction (XRD), respectively. The results indicate that the reactant concentration did not have an obvious influence on the particle size and morphology of LDH, while the composition and crystalline structure were changed to some extent. The corresponding reasons were interpreted deeply. The chloride absorption behavior was investigated, and the powder after immersion in NaCl solutions with different concentrations was characterized by XRD to explain the difference in chloride adsorption amounts. The MgAl-LDH powder synthesized at higher concentrations presented excellent chloride adsorption ability with a Qm value of 155.88 mg/g, which was much better than that reported in the literature. This work demonstrated the superior chloride adsorption of the synthesized MgAl-LDH, and it is of great significance for providing a solid foundation and guidance for the industrial application of LDH in the field of corrosion protection in the future.

Keywords: layered double hydroxide; anion exchange; chloride adsorption; mechanism

check for updates

Citation: Cao, Y.; Fang, S.; Chen, K.; Qi, H.; Zhang, X.; Huang, C.; Wang, J.; Liu, J. Insight into the Preparation of MgAl-Layered Double Hydroxide (LDH) Intercalated with Nitrates and Chloride Adsorption Ability Study. *Appl. Sci.* **2022**, *12*, 4492. https://doi.org/10.3390/app12094492

Academic Editor: Ion Sandu

Received: 24 March 2022
Accepted: 25 April 2022
Published: 28 April 2022

1. Introduction

In recent years, layered double hydroxide (LDH) has been widely used in the field of corrosion protection due to its unique layered structure, anion-accommodating capacity, and anion exchange characteristic [1]. Based on the attractive anion-accommodating capacity of LDH, a wide range of various inhibitors has been intercalated in its gallery. Upon contact with corrosive medium, the loaded inhibitor anions would participate in the anion exchange reaction between them and the aggressive anions in the environment such as Cl^- and SO_4^{2-} [2]. As a result, the aggressive anions were adsorbed into the gallery

of LDH, and the inhibitor anions were released out into the environment, presenting a dual function including reducing the concentration of aggressive chlorides and releasing corrosion inhibitors in this case. The released inhibitor is able to prevent the corrosion of initiation, propagation, and development [3]. On one hand, the self-healing property can be attributed to the enhanced physical barrier effect by filling pores with corrosion products after initiation of corrosion. On the other hand, it is of great significance that the release of inhibitor anions in the defect sites is able to inhibit the development of corrosion by passivation, complexing, and precipitation [4].

One significant application of LDH in the field of anticorrosion is the incorporation of LDH powders as fillers in the organic coatings applied on metal substrates. LDH in coatings is able to absorb chlorides through an anion exchange reaction, resulting in the decrease in the chloride concentration and the release of corrosion inhibitors in the system. In addition, the intercalated chlorides in the gallery were able to further prevent the permeation of chlorides by acting as a concentration gradient wall as shown in Figure 1.

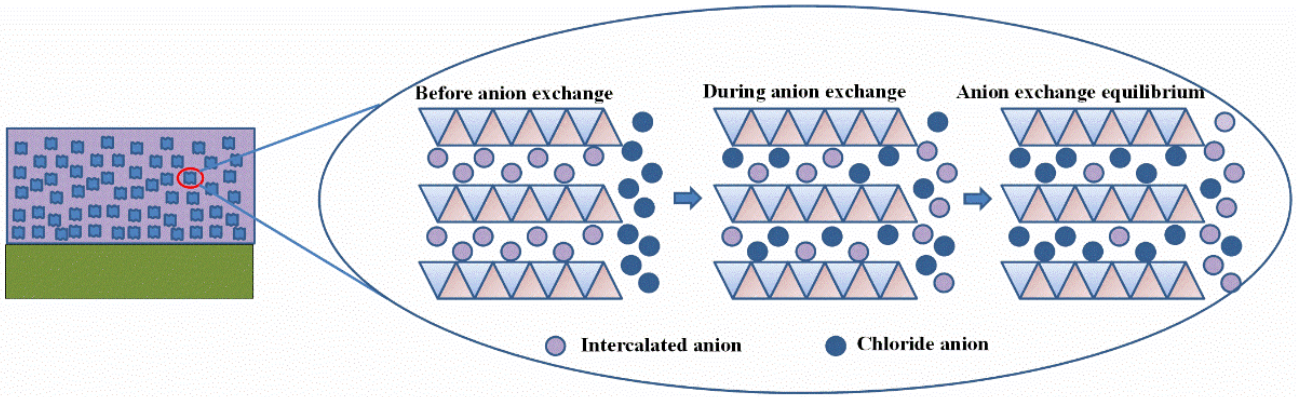

Figure 1. Schematic illustration of working mechanism of LDH used in the anticorrosive coatings.

In the published literature, many researchers focused on the modification of LDH using inhibitors, and enhanced corrosion protection effect was obtained. For example, Su et al. prepared nitrite-intercalated MgAl-LDH and added it into the epoxy coating, and the localized electrochemical impedance spectroscopy (LEIS) test results indicated that the coatings containing LDH-NO_2 presented the most significant corrosion resistance upon the presence of scratches in comparison with the blank coating and the coating with LDH-CO_3 [5]. Alibakhshi et al. reported the application of MgAl-LDH-PO_4^{3-} in a silane primer top-coated by epoxy–polyamide on mild steel. The electrochemical results verified its active corrosion protection ability due to the release of PO_4^{3-} [6]. Li et al. synthesized nitrate and molybdate intercalated ZnAl-LDH, and the controlled release of NO_2^- and MoO_4^{2-} resulted in a relatively long-term corrosion effect [7]. In addition, an environmentally friendly corrosion inhibitor aspartic acid (ASP) was used to modify MgAl-LDH films on Mg alloys by a one-step hydrothermal method by Chen et al. It can be seen that the MgAl-LDH-ASP coating presented an excellent self-healing ability due to the synergistic effect between ASP and the laminate structure of LDH [8]. Ma et al. prepared MgAl-LDH loaded with 5-aminoindazole (AIA), which displayed a controllable release behavior and excellent anticorrosion performance on copper in a 3.5 wt.% NaCl solution [9].

It can be concluded that most of the reported literature paid lots of attention to the modification of LDH with inhibitors, and the inhibitor releasing behavior was studied systematically, while the corresponding chloride adsorption behavior and capacity lack systematic investigation. It should be noted that the inhibitor loading content was closely related with the chloride adsorption capability based on the anion exchange mechanism. Therefore, the optimization of the chloride adsorption capacity before modification would play a positive role in improving the inhibitor loading amount. In this work, the MgAl-LDH intercalated with nitrates was synthesized, and the influence of reactant concentration on

its morphology, composition, structure, and chloride adsorption behavior was investigated comprehensively. The novelty of the research focuses on the relationship of preparation, structure, and properties by investigating the influence of reactant concentration on the structure and chloride adsorption property. The structure, composition, and morphology of the LDH products prepared with different reactant concentrations were systematically characterized to find out the relationship of preparation, structure, and properties. This study is able to provide useful information for industrial preparation of LDH with a strong chloride ability and anticorrosion properties.

2. Materials and Methods

2.1. Materials and Agents

Chemical agents including $Mg(NO_3)_2 \cdot 6H_2O$, $Al(NO_3)_3 \cdot 9H_2O$, NaCl, NaOH, and $NaNO_3$ were provided by Sinopharm Chemical Reagent Co., Ltd. (Shanghai, China) All the agents were analytical grade, and all the solutions were prepared with deionized water.

2.2. Preparation of LDH

MgAl-LDH was prepared by coprecipitation method followed by hydrothermal treatment. A total of 200 mL solution including 0.5 mol/L $Mg(NO_3)_2$ and 0.25 mol/L $Al(NO_3)_3$ was dropped to 2 mol/L $NaNO_3$ (with 3 mol/L NaOH) slowly with rigorous stirring. The temperature of the coprecipitation was kept at 65 °C, and this coprecipitation process lasted 1 h approximately. Then, the LDH slurry was transferred to a stainless hydrothermal reactor for subsequent hydrothermal treatment for 24 h at 120 °C. The product was washed using deionized water by centrifugation and then dried in oven at 60 °C for 48 h. The final obtained sample was labeled as C-high. Another sample labeled as C-low was synthesized according to the above procedure, where the concentration of $Mg(NO_3)_2$, $Al(NO_3)_3$, and $NaNO_3$ was adjusted to 0.25 mol/L, 0.125 mol/L, and 1 mol/L, respectively.

2.3. Characterization of LDH

The morphology of LDH was observed by scanning electron microscopy (SEM, ZEISS ULTRA55) and transmission electron microscopy (TEM, JEM2100). The elemental composition of LDH was characterized by energy dispersive spectrometer (EDS), and chemical composition was obtained by Fourier transform infrared spectroscopy (FTIR, Nicolet IS10). The scanning range was from 4000 cm^{-1} to 700 cm^{-1}, and the resolution was 4 cm^{-1}. Diamond was used as the crystal, and 16 scans were performed. In addition, the chemical composition was also obtained by X-ray photoelectron spectroscopy (XPS, PHI5000 VersaProbe III) using Al Kα source (1486.6 eV). The XPSPEAK 4.1 was used for peak fitting. The X-ray beam adopted high power mode (100 W, 20 kV), and the analysis area was 100 μm × 1400 μm. The spectrum was corrected by shifting C 1s to 248.4 eV. X-ray diffraction (XRD, X'Pert PRO) test using Cu Kα radiation (λ = 1.5406 Å) was carried out in the scanning range from 5 to 80° to characterize the crystalline structure of LDH. The applied voltage was 40 kV, and the current was 40 mA.

2.4. Chloride Adsorption Behavior of the Synthesized LDH Powders

NaCl solutions measuring 0.002, 0.005, 0.01, 0.02, 0.04., and 0.08 mol/L were prepared for the chloride adsorption behavior characterization of LDH. A total of 1 g/100 mL (10 g/L) LDH powder was added into the above solutions. The equilibrium was attained after rigorous stirring of 24 h, and a home-made Ag/AgCl probe by anodization was used for detection of the chloride concentration. The preparation procedure of home-made chloride electrode was described in details as follows: Ag wire (Φ 0.5 mm, 99.99%) was subjected to constant current anodizing in 0.1 mol/L HCl solution with a current density of 0.1 mA/cm^2 for 12 h under dark environment. The reduction of chloride was calculated based on the standard curve.

3. Results and Discussion

3.1. Characterization of LDH Powder

3.1.1. Morphology

The morphology was characterized by SEM as shown in Figure 1. It can be seen that both the two samples C-high and C-low presented three different zones in the SEM images as shown in Figure 2(a1,a2), where zone A,D corresponded to dark area, zone B,E corresponded to light area, and zone C,F corresponded to aggregates. These three different zones were enlarged at high magnifications in Figure 2(b1–d1,b2–d2), respectively. Figure 2(b1,b2) showed uniform and dense distribution of the LDH platelets on the substrates, while Figure 2(c1,c2) showed sparse and sporadic distribution. For Figure 2(d1,d2), the LDH platelets aggregated seriously. The size distribution in Figure 3 also suggested serious aggregation phenomenon, which was in good accordance with the SEM result. It can be seen that both the LDH platelets synthesized at a high or low concentration presented the typical hexagonal shape (Figure 4), which was in good accordance with the literature [5,10–12]. According to inset images, the width (L) and the thickness (d) of the hexagon of C-high in Figure 2(b1) were found to be 118 ± 15 μm and 17.2 ± 3.1 μm, respectively, where the corresponding data for C-low in Figure 2(b2) were found to be 120 ± 20 μm and 19.0 ± 3.4 μm, respectively. It is clear that the change of reactant concentration did not have an obvious influence on the morphology and size of the synthesized LDH platelets.

TEM characterization was also carried out to show more details. It is clear that the LDH platelets possessed a hexagonal shape as shown in the SEM results. The observed lattice spacing in the high resolution TEM in Figure 5c,f indicated good crystallinity of the synthesized LDH [13]. The Fast Fourier Transform (FFT) image further confirmed the good crystallinity.

3.1.2. Structure

XRD characterization was performed to present the crystalline structure of the synthesized samples. The result is shown in Figure 6. It can be seen that both the two samples present the typical structure of LDH, including the (003), (006), (012), (015), (018), (110), (113), and (1310) planes. It is worth noting that the position of the planes of the two samples differs obviously. The (003) and (006) planes of C-high appeared at 9.97° and 19.93°, respectively. In addition, the peak related to the (011) plane of MgO also appeared at 29.48° in the XRD spectrum of this sample. The (003) and (006) planes of C-low appeared at 11.10° and 22.34°, respectively. The interlayer distance of C-high and C-low can be calculated to be 8.87 Å and 7.96 Å according to the position of the (003) plane and Bragg's Law, corresponding to the intercalated NO_3^- and CO_3^{2-}/OH^-, respectively [14–16]. The underlying reason for this difference may be that a lower concentration of Mg^{2+} and Al^{3+} reacted with less hydroxyls in the case of C-low coprecipitation; as a result, the concentration of remained hydroxyls in the solution would be higher. The pH after the coprecipitation in the case of C-high and C-low was measured to be 8.0 and 12.7, respectively, which supported the above explanation powerfully. A higher pH usually involves more carbonate contamination in the preparation, and instead of nitrates, more CO_3^{2-}/OH^- would be intercalated in the LDH gallery, leading to the position shift of the planes towards higher 2θ angles [17,18]. In addition, a higher pH may have obvious influence on the formation of $Al(OH)_3$ and $Mg(OH)_2$, thus the structure of the finally obtained MgAl-LDH would probably be different.

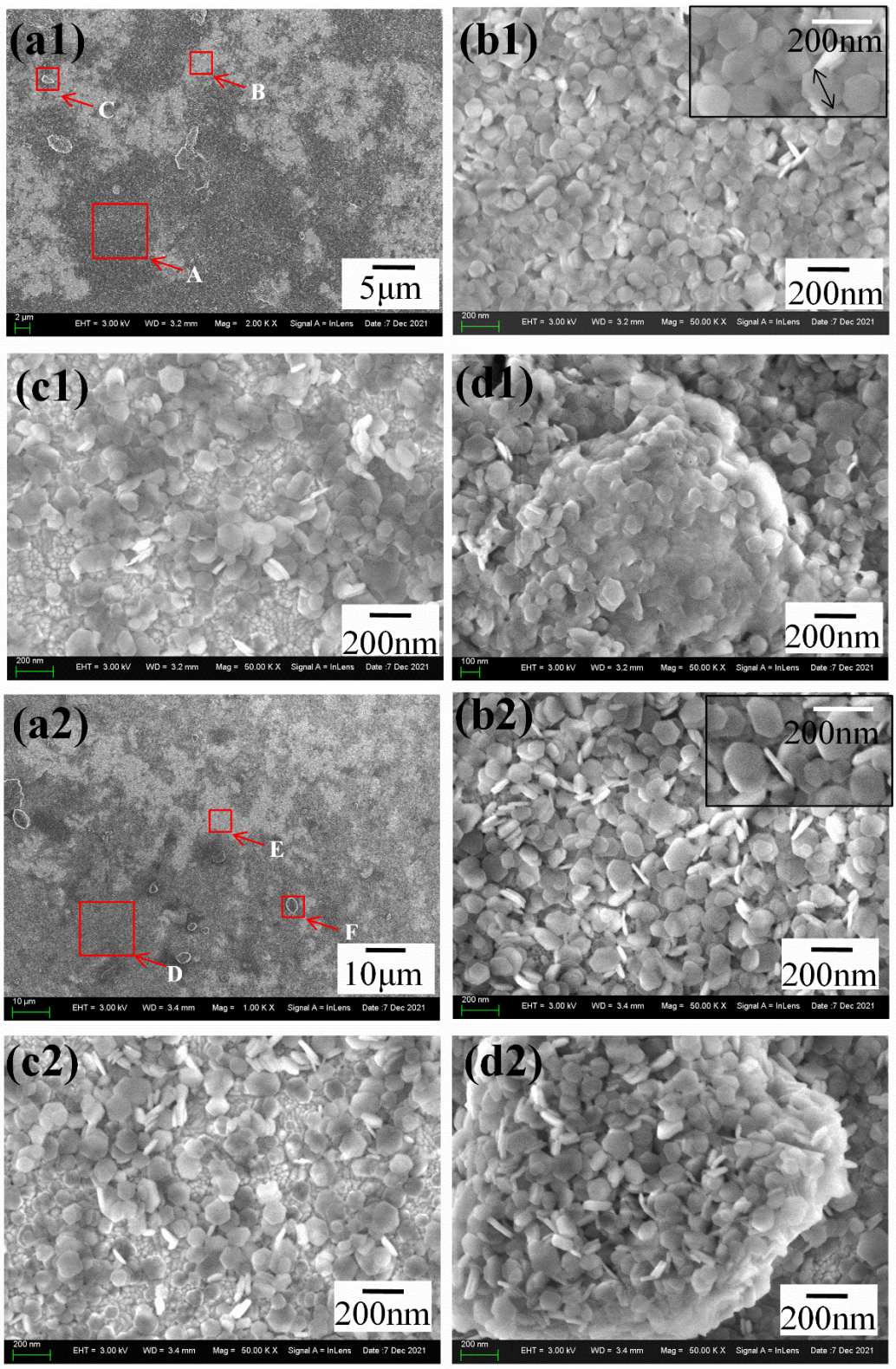

Figure 2. The SEM images of sample C-high (**a1**–**d1**) and C-low (**a2**–**d2**) (Please note that (**b1**,**c1**,**d1**) corresponded to the magnified images of zones A, B, and C in (**a1**); (**b2**,**c2**,**d2**) corresponded to the magnified images of zones D, E, and F in (**a2**)).

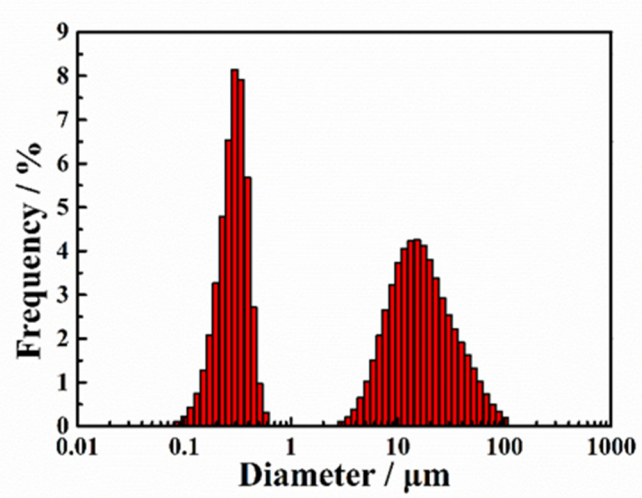

Figure 3. Size distribution of LDH.

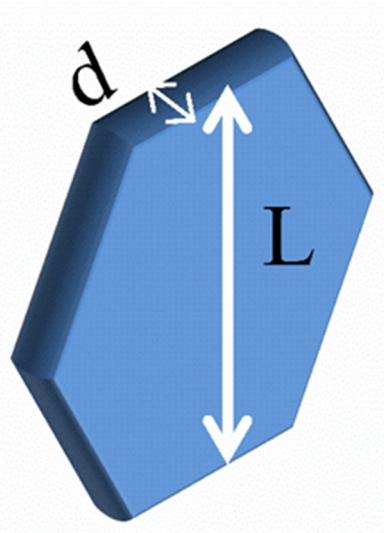

Figure 4. Schematic illustration of hexagonal LDH platelet.

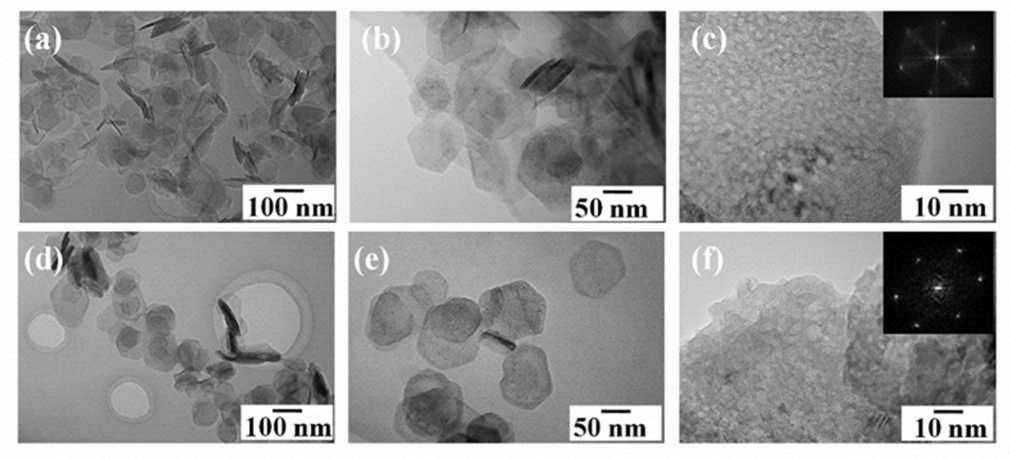

Figure 5. The TEM images of sample C-high (**a**–**c**) and C-low (**d**–**f**) (Please note that the inset images in (**c**,**f**) were the Fast Fourier Transform (FFT) image).

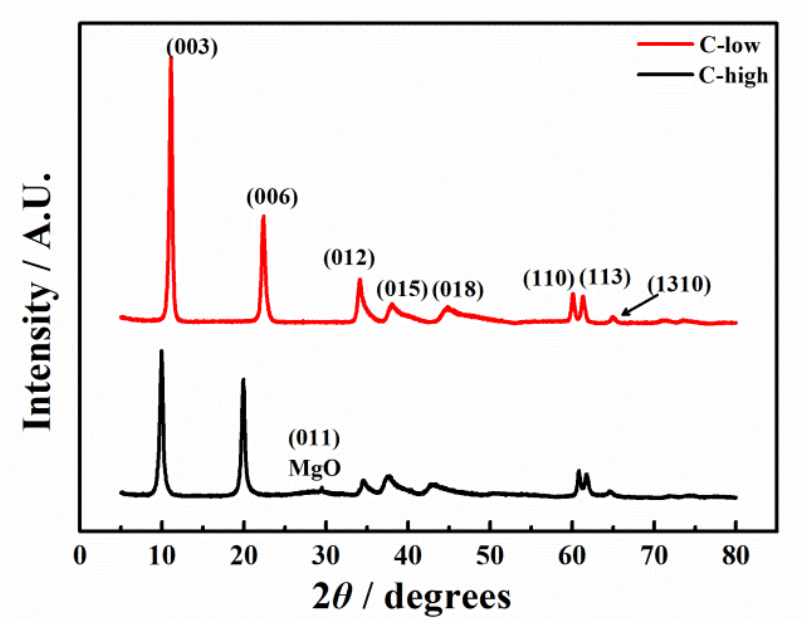

Figure 6. The XRD result of the synthesized samples.

3.1.3. Composition

The elemental information of the prepared samples characterized by EDS is shown in Figure 7, and the atomic percentage of various elements is displayed in Table 1. According to this table, C element accounted for an obviously higher percentage in C-low than that in C-high, which was caused by the intercalation of a larger number of carbonates in C-low. This result was in good accordance with the XRD result above. As for the O element, the atomic percentage was 68.40% in C-high and 62.59% in C-low, respectively. It can be seen that the atomic percentage of O in these two samples was close to each other, and remarkable differences cannot be observed. It can be seen that the Mg/Al ratio differed greatly between the C-high and C-low samples. This value was 1.88 ± 0.07 for C-high, and it was close to the ratio of Mg/Al in the reactant. However, this value increased to 2.79 ± 0.16 when the reactant concentration was reduced. This result indicates that different MgAl-LDH was formed when the reactant concentration was changed. As explained above, the difference in pH value in the synthesis process of the two samples may result in this observation. According to the literature, the change of M^{2+}/M^{3+} ratio did not have an influence on the position of the (003) plane, and thus the difference in C-high and C-low in terms of the (003) plane position can only be attributed to the difference in intercalated anions [19]. In addition, the elemental distribution and the atomic percentage of different elements in the samples of C-high and C-low are shown in Figure 8, and it can be seen that the various elements including C, O, Mg, and Al were distributed uniformly, verifying the formation of MgAl-LDH instead of a mixture of oxides or hydroxides of magnesium and aluminum.

The FTIR spectra are shown in Figure 9. The broad peak occurring in the range of 3000–3700 cm^{-1} of the two samples can be attributed to the hydroxyl group in LDH and the adsorbed water molecules. The two peaks around 2300 cm^{-1} were related to the asymmetric stretching vibration of CO_2 in the atmosphere. The peak at 1645 cm^{-1} was due to the bending vibration of water molecules. The adsorption peaks below 1000 cm^{-1} can be assigned to the lattice vibrations and stretching modes of M–O and M–OH (M refers to Mg^{2+} and Al^{3+}) [15]. For the sample of C-high, the peak at 1355 cm^{-1} with a shoulder peak at higher wavenumber can be attributed to the cointercalated nitrates and carbonates. The peak at 1362 cm^{-1} can be assigned to the intercalated carbonates in the sample of C-low.

Furthermore, an XPS test was carried out to demonstrate more detailed information related to chemical bonds. As can be seen from Figure 10a, the survey spectra of the two samples were similar to each other and indicated the presence of Mg, Al, C, N, and O. The high-resolution XPS spectra of N at 407.2 eV for C-high and 407.0 eV for C-low can be attributed to nitrates, indicating that nitrates existed in both samples. It should be noted that the signal of N element of C-high was obviously much stronger with less noise in comparison with that of C-low. The C 1s XPS spectrum for C-high consisted of two components including ubiquitous contaminant carbon at 284.8 eV and C=O group of CO_3^{2-} at 288.6 eV [15]. The C 1s spectrum for C-low also contained two peaks appearing at 248.8 eV and 287.7 eV. The slight shift of C=O may be related to a different environment caused by a different pH in the synthesis. The O 1s XPS spectrum of C-high included three peaks, corresponding to H_2O at 533.1 eV, NO_3^- at 532.4 eV, and CO_3^{2-} or $Al(OH)_3$ at 531.8 eV [20]. For the C-low sample, the peak at 532.3 eV can be attributed to NO_3^-; the peak at 531.6 eV can be attributed to CO_3^{2-}, and the peak at 530.9 eV was due to $Mg(OH)_2$ [21]. According to Figure 10f,g, it is clear that more carbonates appeared in the sample of C-low than that of sample C-high, which was in good agreement with the EDS result, FTIR result, and XRD result. The XPS result further complemented the information related to LDH composition and demonstrated the difference in terms of the carbonate and nitrate numbers in the LDH gallery between the two samples. It can be concluded that the sample C-high contained more nitrates and fewer carbonates, while it was the opposite in the case of C-low.

Table 1. The atomic percentage of various elements and Mg/Al ratio in the samples of C-high and C-low.

Element (At.%)	C	O	Mg	Al	Mg/Al Ratio
C-high	13.97 ± 1.36	68.40 ± 0.70	11.49 ± 0.43	6.13 ± 0.32	1.88 ± 0.07
C-low	23.64 ± 1.63	62.59 ± 0.84	10.11 ± 0.69	3.66 ± 0.10	2.79 ± 0.16

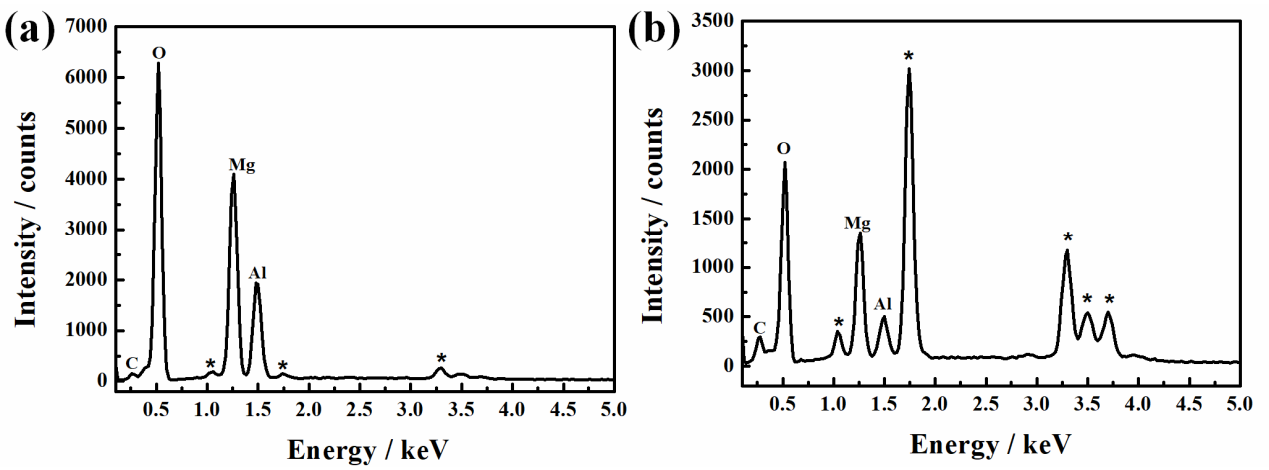

Figure 7. The EDS result of (**a**) C-high and (**b**) C-low (Please note that * means elements from the ITO substrate and the contaminants).

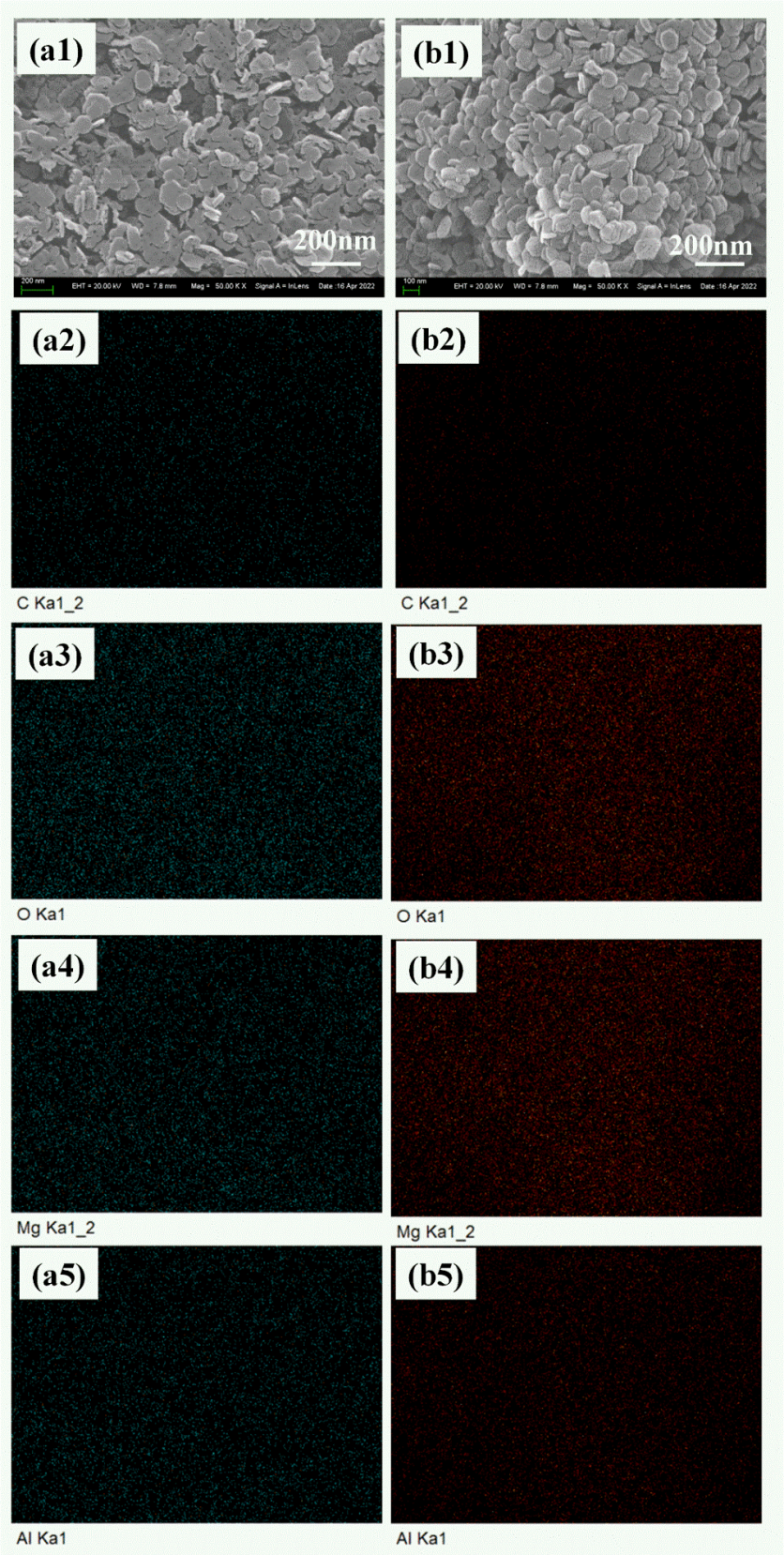

Figure 8. The elemental distribution of different elements in the samples of C-high (**a1**–**a5**) and C-low (**b1**–**b5**).

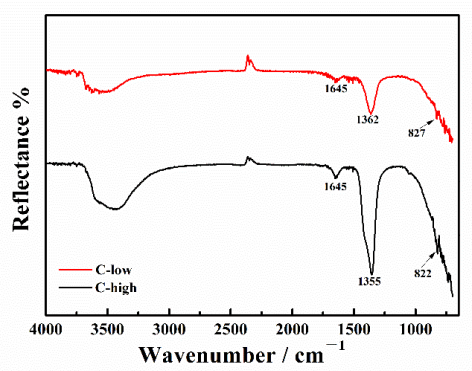

Figure 9. The FTIR results of the synthesized samples.

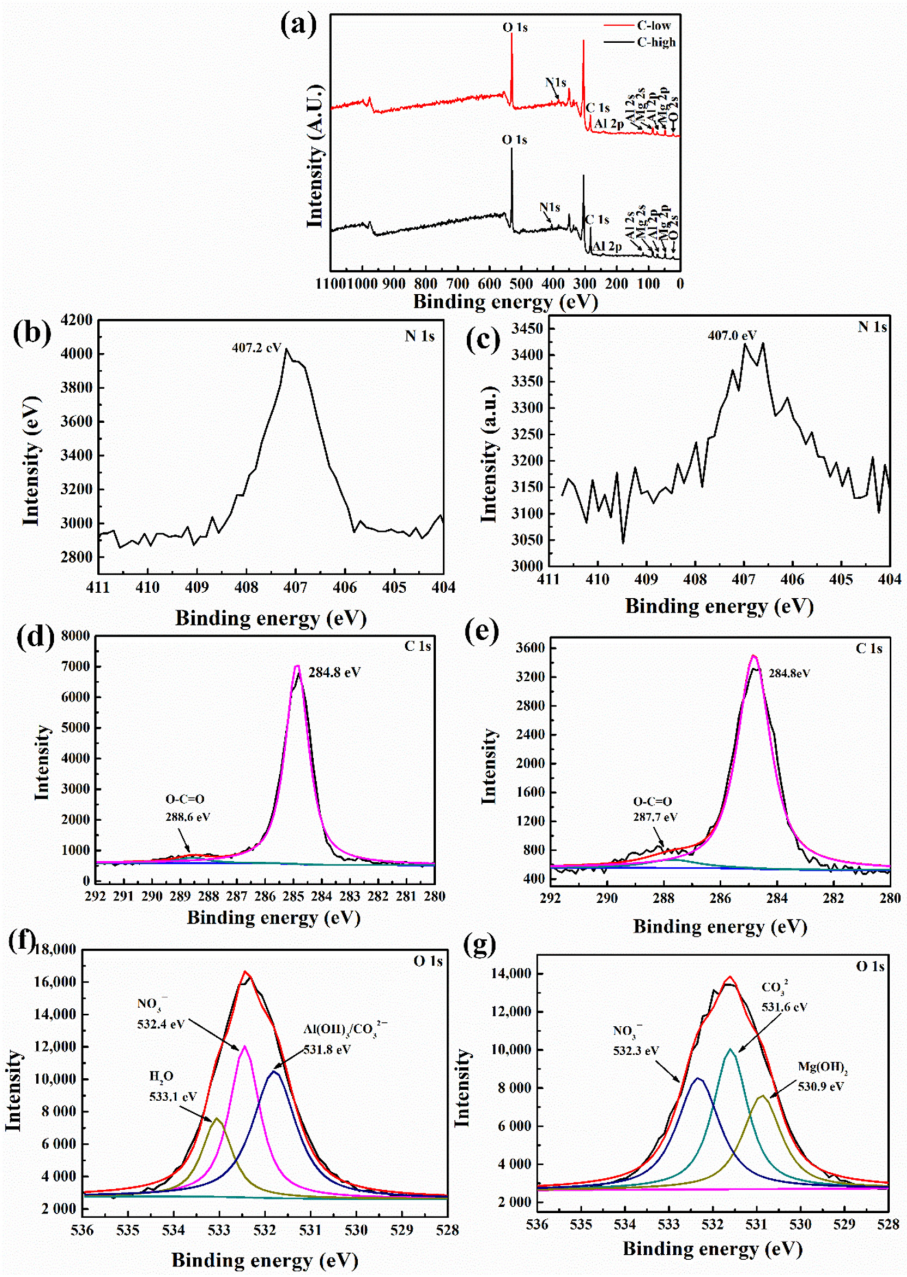

Figure 10. (**a**) XPS survey spectra of the two synthesized samples. High-resolution XPS spectra of sample C-high; (**b**) N 1s, (**d**) C 1s, (**f**) O 1s, and sample C-low (**c**) N 1s, (**e**) C 1s, and (**g**) O 1s.

3.2. Chloride Adsorption Behavior of LDH

Chloride is the most common aggressive anion in a corrosive medium, and the concentration of chloride in the solution has a significant influence on the corrosion of metals; therefore, in this manuscript, the chloride adsorption property of LDH was investigated. In order to characterize the chloride adsorption behavior of LDH and obtain the amount of chloride adsorption at equilibrium (mg/g), 1 g LDH was added to 100 mL of a different NaCl solution and subjected to rigorous magnetic stirring for 24 h. The pH of the NaCl solution before the addition of LDH was measured to be 7.2, while the pH of NaCl solutions with a concentration of 0.02 mol/L rose to 8.8 and 8.9 after 24 stirring with C-high and C-low, respectively. This slight increase in pH can be attributed to the release of OH^- anions from the LDH gallery by the anion exchange reaction between OH^- and chlorides. The remaining chloride concentration was measured, and the chloride reduction percentage was calculated, which is shown in Figure 11a. As can be seen from this figure, the reduction percentage increased from 40% to 55% gradually when the NaCl concentration was increased from 0.002 to 0.04 mol/L, and it decreased to 34% when the NaCl concentration was further increased to 0.08 mol/L. For the sample C-low, the reduction percentage was 25% when the NaCl solution was 0.002 mol/L, and it decreased gradually to about 1% when the NaCl concentration increased to 0.01 mol/L. With the further increase in NaCl concentration, the reduction percentage was around 0%, which was probably caused by the relatively lower sensitivity of the Ag/AgCl probe at a higher chloride concentration. This result indicates the poor chloride adsorption ability of C-low. This result may be probably caused by the existence of a large number of carbonates in its gallery and the low adsorption capacity of LDH itself. According to the XRD results in Figure 6, the amount of CO_3^{2-} in the gallery of C-low was remarkably higher than that of C-high. As carbonates have a strong affinity with the interlayer, it is hard for the chlorides in the solution to replace carbonates in the LDH gallery by an anion exchange reaction. As a result, the chloride adsorption ability of C-low was found to be much lower than that of C-high. The chloride uptake amount of LDH was calculated according to Equation (1) [22]:

$$Q_e = \frac{1000(C_0 - C_e)VM}{m} \tag{1}$$

where Q_e is the amount of chloride adsorption at the equilibrium (mg g^{-1}), and C_0 and C_e are the initial and equilibrium chloride concentration (mol/L), respectively. V is the solution volume (L); M is the molar mass of Cl element with a value of 35.5 mol/g, and m is the mass of LDH (g). The Q_e of LDH in different NaCl solutions is shown in Figure 11b. It can be seen that Q_e of C-high increased remarkably from 2.84 to 97.63 mg g^{-1} when the NaCl concentration was increased from 0.002 mol/L to 0.08 mol/L. In the case of C-low, Q_e remained at 1.78 mg g^{-1} when the NaCl solution increased from 0.002 to 0.005 mol/L, demonstrating that the chloride adsorption ability was maximized at a low concentration at 0.002 mol/L. As explained above, the Q_e stayed around 0 mg g^{-1} when the NaCl concentration further increased due to the lower sensitivity of the Ag/AgCl probe at a higher NaCl concentration. Based on the above analysis, it can be concluded that the sample C-high possessed superior chloride adsorption ability in comparison with the sample of C-low.

According to the literature, the Langmuir isotherm can provide better fitting for the chloride adsorption by LDH; therefore, the Langmuir isotherm (Equation (2)) was used for fitting in this work [22].

$$Q_e = \frac{K_L Q_m C_e}{1 + K_L C_e} \tag{2}$$

where K_L (L mol^{-1}) is related to the binding energy, and Q_m (mg g^{-1}) means the maximum amount of chloride adsorption per unit mass of LDH for monolayer coverage. Q_e is the amount of chloride adsorption at the equilibrium (mg g^{-1}), and C_e is the chloride concentration at equilibrium (mol/L). The fitting result of C-high is shown in Figure 12. K_L

was 36.16 L mol^{-1}, and Q_m was 155.88 mg g^{-1}. The value of Q_m was much higher than that reported in most of the literature [22–24]. The comparison with the literature in terms of Q_m is shown in Table 2.

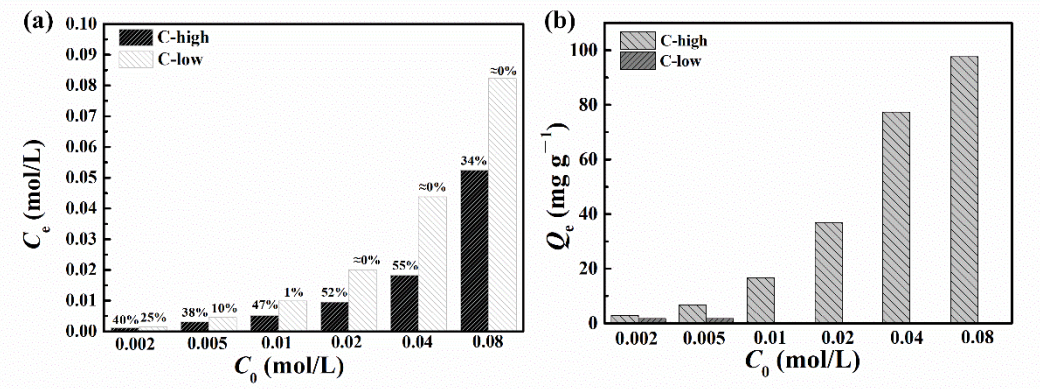

Figure 11. (**a**) The chloride concentration after chloride adsorption for 24 h and chloride reduction percentage of sample C-high and C-low in different NaCl solutions; (**b**) The amount of chloride adsorption at the equilibrium (mg g^{-1}) in different NaCl solutions.

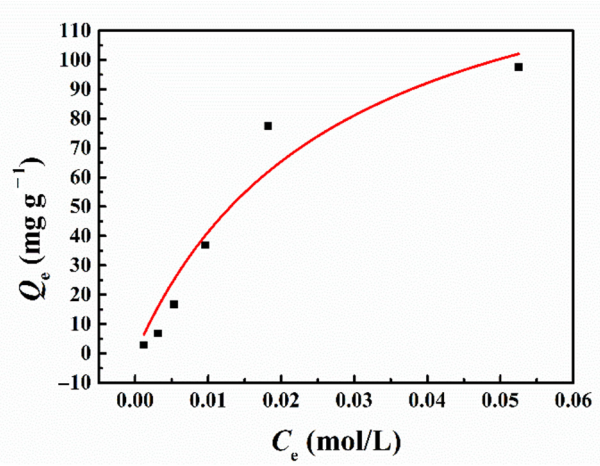

Figure 12. Langmuir isothermal curve for chloride adsorption reaction of C-high.

Table 2. The comparison with the literature in terms of Q_m.

LDH	Q_m (mg g^{-1})	Literature
MgAl-LDH-NO_3^-	155.88	Our work
MgAl-LDH-pAB	33.54	22
MgAl-LDH-NO_3^-	107.00	23
MgAl-LDH-NO_2^-	88.75	23
MgAl-LDH-NO_3^-	111.29	24
CaAl-LDH-NO_3^-	115.55	24
ZnAl-LDH-NO_3^-	148.28	24

The LDH after anion exchange reaction in different NaCl solutions was characterized by XRD in order to investigate the detailed chloride adsorption process and to provide an explanation for the different chloride adsorption capacities of C-high and C-low shown above. As can be seen from Figure 13a, the peak of the (003) plane appeared at 10.04°, 10.11°, 10.13°, 10.73°, 11.52°, and 11.58° when the NaCl solution was 0.002, 0.005, 0.01, 0.02, 0.04, and 0.08 mol/L, respectively. With the right shift of 2θ degrees, the interlayer anions changed from nitrates to chlorides gradually, indicating that more chlorides were loaded in the LDH interlayer when the NaCl concentration increased. Therefore, the chloride

adsorption amount increased as shown in Figure 11 and Table 2. The XRD result of C-low after immersion in different NaCl solutions is shown in Figure 13b. It can be seen that the (003) plane occurred at around 11.20°, mainly corresponding to the intercalated carbonates in the coprecipitation process. This verifies the explanation for the weak chloride adsorption property of C-low stated above.

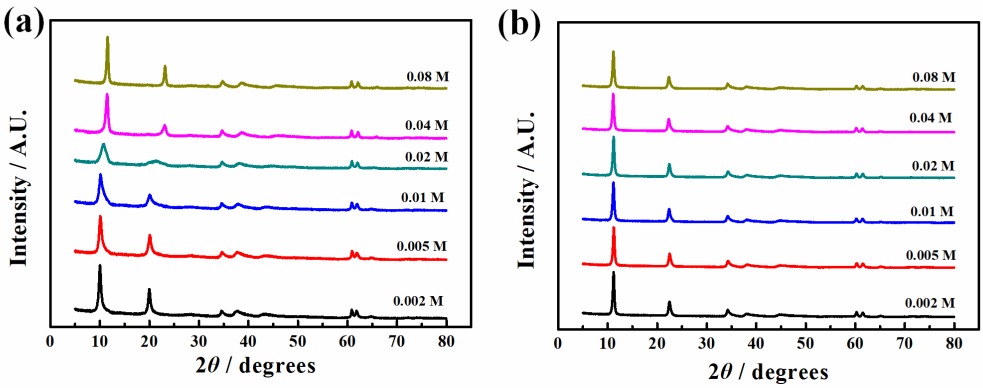

Figure 13. The XRD results of C-high (**a**) and C-low (**b**) after immersion in various NaCl solutions for 24 h.

It should be noted that the adsorption of chlorides by LDH is mainly dependent on the anion exchange reaction between the intercalated anion in the LDH gallery and the aggressive chlorides in the environment, thus the propensity of the anion exchange reaction has a dominant influence on the adsorption ability of chlorides. Based on our results, more carbonates were intercalated in the LDH gallery of C-low than that of C-high, and they are difficult to replace by chlorides due to their strong affinity with the interlayer; therefore, C-low presented a much lower adsorption ability in comparison with C-high.

The FTIR characterization of C-high and C-low after immersion in various NaCl solutions for 24 h was also carried out. The results are shown in Figure 14. In Figure 14a, the two peaks corresponding to carbonates and nitrates appeared in the FTIR spectrum of C-high. It can be seen that the peak corresponding to nitrates almost disappeared after immersion in the 0.08 M NaCl solution for 24 h due to the almost complete anion exchange reaction in the case of C-high, while the peak corresponding to carbonates in the FTIR spectrum of C-low in Figure 14b did not change remarkably in various NaCl solutions due to the difficulty of anion exchange reaction between carbonate ions in the LDH gallery and the chlorides in the environment. This result is in perfect accordance with the XRD result in Figure 13.

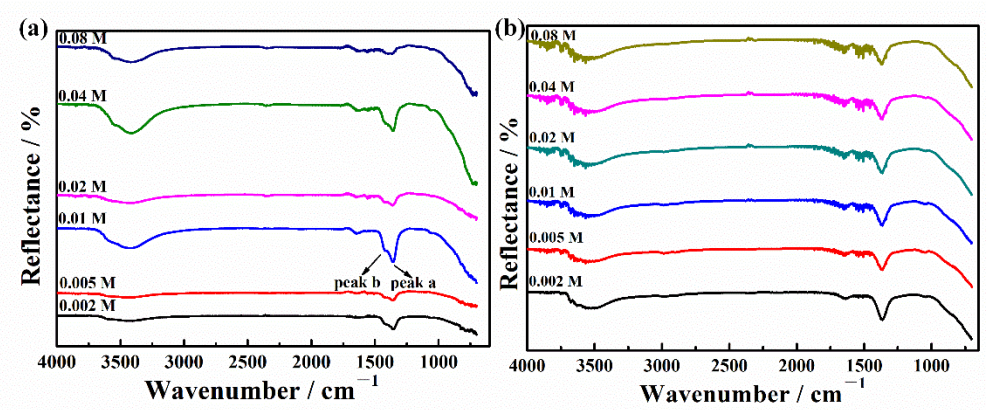

Figure 14. The FTIR results of C-high (**a**) and C-low (**b**) after immersion in various NaCl solutions for 24 h.

4. Conclusions

In this work, MgAl-LDH intercalated with nitrates was prepared by coprecipitation. The influence of the reactant concentration on the formation of LDH was investigated. The following points of conclusions can be obtained:

(1) The change of reactant concentration hardly had an influence on the morphology and size of the LDH platelets, while the pH difference caused by different metal ion concentrations may have a remarkable effect on the intercalated anions. The difference in reactant concentration resulted in the change of pH value of the reactant solution. An obviously higher pH with a value of 12.7 in the case of C-low leads to the intercalation of a larger number of carbonates, resulting in a lower chloride adsorption capability due to the difficulty of anion exchange reaction. This finding emphasizes the importance of pH value in LDH synthesis, which can be easily ignored when other conditions were changed. pH should be controlled well during the LDH synthesis process to guarantee the quality of the synthesized LDH. This result could provide meaningful guidance into further preparation of MgAl-LDH.

(2) The sample of C-high presents superior chloride adsorption ability with a Q_m value of 155.88 mg g^{-1}, which was much better than that reported in the literature. This work is able to provide a solid foundation for the production of LDH with a strong chloride adsorbing property and further industrial application in the field of corrosion protection in the future.

Author Contributions: Conceptualization, Y.C. and K.C.; Methodology, H.Q.; Software, X.Z.; Validation, Y.C., H.Q. and S.F.; Formal Analysis, S.F.; Investigation, Y.C.; Resources, K.C.; Data Curation, S.F.; Writing—Original Draft Preparation, Y.C.; Writing—Review and Editing, J.W.; Visualization, J.L.; Supervision, J.W.; Project Administration, C.H.; Funding Acquisition, H.Q. All authors have read and agreed to the published version of the manuscript.

Funding: This research was funded by State Key Laboratory for Marine Corrosion and Protection Foundation (JS220902).

Institutional Review Board Statement: Not applicable.

Informed Consent Statement: Not applicable.

Data Availability Statement: The data presented in this study are available on request from the corresponding author.

Acknowledgments: Dichun Chen is acknowledged for his help in TEM characterization.

Conflicts of Interest: The authors declare no conflict of interest.

References

1. Cao, Y.; Zheng, D.; Zhang, F.; Pan, J.; Lin, C. Layered double hydroxide (LDH) for multi-functionalized corrosion protection of metals: A review. *J. Mater. Sci. Technol.* **2022**, *102*, 232–263. [CrossRef]
2. Zheludkevich, M.L.; Tedim, J.; Ferreira, M.G.S. "Smart" coatings for active corrosion protection based on multi-functional micro and nanocontainers. *Electrochim. Acta* **2012**, *82*, 314–323. [CrossRef]
3. Zhang, Y.; Liu, J.; Li, Y.; Yu, M.; Li, S.; Xue, B. Fabrication of inhibitor anion-intercalated layered double hydroxide host films on aluminum alloy 2024 and their anticorrosion properties. *J. Coat. Technol. Res.* **2015**, *12*, 293–302. [CrossRef]
4. Zhang, F.; Ju, P.; Pan, M.; Zhang, D.; Huang, Y.; Li, G.; Li, X. Self-healing mechanisms in smart protective coatings: A review. *Corros. Sci.* **2018**, *144*, 74–88. [CrossRef]
5. Su, Y.; Qiu, S.; Yang, D.; Liu, S.; Zhao, H.; Wang, L.; Xue, Q. Active anti-corrosion of epoxy coating by nitrite ions intercalated MgAl LDH. *J. Hazard. Mater.* **2020**, *391*, 122215. [CrossRef]
6. Alibakhshi, E.; Ghasemi, E.; Mahdavian, M.; Ramezanzadeh, B.; Farashi, S. Active corrosion protection of Mg-Al-PO_4^{3-} LDH nanoparticle in silane primer coated with epoxy on mild steel. *J. Taiwan Inst. Chem. Eng.* **2017**, *75*, 248–262. [CrossRef]
7. Li, W.H.; Tian, H.W.; Wang, D.P. Controlled Release of Nitrate and Molybdate Intercalated in Zn-Al-Layered Double Hydroxide Nanocontainers towards Marine Anticorrosion Applications. *Colloid Interfac. Sci.* **2018**, *24*, 18–23. [CrossRef]
8. Chen, J.; Fang, L.; Wu, F.; Xie, J.; Hu, J.; Jiang, B.; Luo, H. Corrosion resistance of a self-healing rose-like MgAl-LDH coating intercalated with aspartic acid on AZ31 Mg alloy. *Prog. Org. Coat.* **2019**, *136*, 105234. [CrossRef]

9. Ma, L.; Qiang, Y.; Zhao, W. Designing novel organic inhibitor loaded MgAl-LDHs nanocontainer for enhanced corrosion resistance. *Chem. Eng. J.* **2021**, *408*, 127367. [CrossRef]
10. Goh, K.H.; Lim, T.T.; Dong, Z. Application of layered double hydroxides for removal of oxyanions: A review. *Water Res.* **2008**, *42*, 1343–1368. [CrossRef]
11. Guo, X.; Zhang, F.; Xu, S.; Evans, D.G.; Duan, X. Preparation of layered double hydroxide films with different orientations on the opposite sides of a glass substrate by in situ hydrothermal crystallization. *Chem. Commun.* **2009**, 6836–6838. [CrossRef] [PubMed]
12. Su, Y.; Qiu, S.; Wei, J.; Zhu, X.; Zhao, H.; Xue, Q. Sulfonated polyaniline assisted hierarchical assembly of graphene-LDH nanohybrid for enhanced anticorrosion performance of waterborne epoxy coatings. *Chem. Eng. J.* **2021**, *426*, 131269. [CrossRef]
13. Kosari, A.; Visser, P.; Tichelaar, F.; Eswara, S.; Audinot, J.N.; Wirtz, T.; Zandbergen, H.; Terryn, H.; Mol, J.M.C. Cross-sectional characterization of the conversion layer formed on AA2024-T3 by a lithium-leaching coating. *Appl. Surf. Sci.* **2020**, *512*, 145665. [CrossRef]
14. Chen, Y.; Wu, L.; Yao, W.; Chen, Y.; Zhong, Z.; Ci, W.; Wu, J.; Xie, Z.; Yuan, Y.; Pan, F.A. self-healing corrosion protection coating with graphene oxide carrying 8-hydroxyquinoline doped in layered double hydroxide on a micro-arc oxidation coating. *Corros. Sci.* **2022**, *194*, 109941. [CrossRef]
15. Hu, T.; Ouyang, Y.; Xie, Z.H.; Wu, L. One-pot scalable in situ growth of highly corrosion-resistant MgAl-LDH/MBT composite coating on magnesium alloy under mild conditions. *J. Mater. Sci. Technol.* **2021**, *92*, 225–235. [CrossRef]
16. Yang, H.; Xiong, C.; Liu, A.; Li, W. The effect of layered double hydroxides intercalated with vitamin B3 on the mechanical properties, hydration and pore structure of cement-based materials. *Mater. Lett.* **2021**, *300*, 130228. [CrossRef]
17. Vieira, D.E.L.; Salak, A.N.; Ferreira, M.G.S.; Vieira, J.M.; Brett, C.M.A. Ce-substituted Mg-Al layered double hydroxides to prolong the corrosion protection lifetime of aluminium alloys. *Appl. Surf. Sci.* **2022**, *573*, 151527. [CrossRef]
18. Alibakhshi, E.; Ghasemi, E.; Mahdavian, M.; Ramezanzadeh, B.; Mana, Y. The effect of interlayer spacing on the inhibitor release capability of layered double hydroxide based nanocontainers. *J. Clean. Prod.* **2020**, *251*, 119676. [CrossRef]
19. Pham, T.T.; Nguyen, T.D.; Nguyen, A.S.; Paint, Y.; Gonon, M.; To, T.X.H.; Olivier, M.G. A comparative study of the structure and corrosion resistance of ZnAl hydrotalcite conversion layers at different Al^{3+}/Zn^{2+} ratios on electrogalvanized steel. *Surf. Coat. Technol.* **2022**, *429*, 127948. [CrossRef]
20. Wu, W.; Sun, X.; Zhu, C.L.; Zhang, F.; Zeng, R.C.; Zou, Y.H.; Li, S.Q. Biocorrosion resistance and biocompatibility of Mg–Al layered double hydroxide/poly-L-glutamic acid hybrid coating on magnesium alloy AZ31. *Prog. Org. Coat.* **2020**, *147*, 105746. [CrossRef]
21. Wu, L.; Ding, X.; Zheng, Z.; Tang, A.; Zhang, G.; Atrens, A.; Pan, F. Doublely-doped Mg-Al-Ce-$V_2O_7^{4-}$ LDH composite film on magnesium alloy AZ31 for anticorrosion. *J. Mater. Sci. Technol.* **2021**, *64*, 66–72. [CrossRef]
22. Wei, J.; Xu, J.; Mei, Y.; Tan, Q. Chloride adsorption on aminobenzoate intercalated layered double hydroxides: Kinetic, thermodynamic and equilibrium studies. *Appl. Clay Sci.* **2020**, *187*, 105495. [CrossRef]
23. Xu, J.; Song, Y.; Zhao, Y.; Jiang, L.; Mei, Y.; Chen, P. Chloride removal and corrosion inhibitions of nitrate, nitrite-intercalated Mg Al layered double hydroxides on steel in saturated calcium hydroxide solution. *Appl. Clay Sci.* **2018**, *163*, 129–136. [CrossRef]
24. Chen, M.; Wu, F.; Yu, L.; Cai, Y.; Chen, H.; Zhang, M. Chloride binding capacity of LDHs with various divalent cations and divalent to trivalent cation ratios in different solutions. *CrystEngComm* **2019**, *21*, 6790–6800. [CrossRef]